Tidal deformability of neutron and hyperon stars within relativistic mean field equations of state

Bharat Kumar,* S. K. Biswal, and S. K. Patra
Institute of Physics, Bhubaneswar 751005, India
and Homi Bhabha National Institute, Training School Complex, Anushakti Nagar, Mumbai 400085, India
(Received 30 September 2016; published 4 January 2017)

We systematically study the tidal deformability for neutron and hyperon stars using relativistic mean field equations of state (EOSs). The tidal effect plays an important role during the early part of the evolution of compact binaries. Although, the deformability associated with the EOSs has a small correction, it gives a clean gravitational wave signature in binary inspiral. These are characterized by various Love numbers k_l ($l = 2, 3, 4$), that depend on the EOS of a star for a given mass and radius. The tidal effect of star could be efficiently measured through an advanced LIGO detector from the final stages of an inspiraling binary neutron star merger.

DOI: 10.1103/PhysRevC.95.015801

I. INTRODUCTION

The detection of a gravitational wave is a major breakthrough in astrophysics/cosmology which is detected for the first time by the advanced Laser Interferometer Gravitational-wave Observatory (aLIGO) detector [1]. Inspiraling and coalescing of a binary black-hole results in the emission of gravitational waves. We may expect that in a few years the forthcoming aLIGO [1], VIRGO [2], and KAGRA [3] detectors will also detect gravitational waves emitted by binary neutron stars (NSs). This detection is certainly posed to be a valuable guide and will help in a better understanding of a highly compressed baryonic system. Flanagan and Hinderer [4–6] have recently pointed out that tidal effects are also potentially measurable during the early part of the evolution when the waveform is relatively clean. It is understood that the late inspiral signal may be influenced by the tidal interaction between binary stars (NS-NS), which gives important information about the equation of state (EOS). The study of Refs. [7–16] inferred that the tidal effects could be measured using the recent generation of gravitational wave (GW) detectors.

In 1911, the mathematician A. E. H. Love [17] introduced the dimensional parameter in Newtonian theory that is related to the tidal deformation of the Earth due to the gravitational attraction between the Moon and the Sun. This Newtonian theory of tides has been imported to the general relativity [12,18], where it shows that the electric and magnetic type dimensionless gravitational Love number is a part of the tidal field associated with the gravitoelectric and gravitomagnetic interactions. The tidal interaction in a compact binary system has been encoded in the Love number and is associated with the induced deformation responded by changing shapes of the massive body. We are particularly interested in a neutron star in a close binary system, focusing on the various Love numbers k_l ($l = 2, 3, 4$) due to the shape changes (like quadrupole, octupole, and hexadecapole in the presence of an external gravitational field). Although higher Love numbers ($l = 3, 4$) give negligible effect, still these Love numbers (k_l) can have vital importance in future gravitational wave astronomy. However, geophysicists are interested to calculate the surficial Love number h_l, which describes the deformation of the body's surface in a multipole expansion [12,18,19].

We have used the equation of state from the relativistic mean field (RMF) [20–22] and the newly developed effective field theory motivated RMF (E-RMF) [23,24] approximation in our present calculations. Here, the degrees of freedom are nucleon, σ, ω, ρ, π mesons, and photon. This theory very well explains the properties of finite nuclei and nuclear matter systems at a higher density region. Walecka has generalized [22] the RMF approximation and then subsequently Boguta and Bodmer [25] extended to the self-interaction of the σ meson to reproduce proper experimental observables. In the E-RMF formalism, all the possible couplings of the mesons among themselves and also their cross-interactions are considered [23,24]. The self- and crossed interactions are very significant. For example, the self-interaction of the σ meson brings back the nuclear matter incompressibility K_∞ from an unacceptably high value of $K_\infty \sim 600$ MeV to a reasonable K_∞ of $\sim$270 MeV [25,26]. Similarly, the quartic self-interaction of the vector meson ω softens the equation of state [27,28]. It is to be noted that all the mesons and their self- and cross-interaction terms in the effective Lagrangian do not need to be included, because of some symmetry and their heavy masses [29]. This theory of dense matter fairly explains the observed massive neutron star, like PSR J1614-2230 with mass $M = 1.97 \pm 0.04 M_\odot$ [30] and PSR J0348+0432 ($M = 2.01 \pm 0.04 M_\odot$) [31].

The baryon octets are also introduced as the stellar system is in extraordinary condition such as highly asymmetric or extremely high density medium [32]. The coupling constants for nucleon-mesons are fitted to reproduce the properties of a finite number of nuclei, which then predict not only the observables of β-stable nuclei, but also of drip-lines and superheavy regions [22,25,28,33–37]. The hyperon-meson couplings are obtained from the quark model [38–40]. Recently, however, the couplings were improved by taking into consideration some other properties of strange nuclear matter [41].

The paper is organized as follows. In Sec. II, we give a brief description on the relativistic mean field (RMF/E-RMF) formalism. The ingredients of the quantum hadrodynamic model (QHD) and resulting EOSs are outlined in this section.

*bharat@iopb.res.in

The various tidal Love numbers and tidal deformability of neutron and hyperon stars are discussed in Secs. III C and III D after describing the numerical scheme. Finally, the summary and concluding remarks are given in Sec. IV.

II. THE RELATIVISTIC MEAN FIELD FORMALISM

The effective field theory motivated relativistic mean field (E-RMF) Lagrangian is designed with underlying symmetries of quantum chromodynamics (QCD) and the parameters of G1 and G2 are constructed taking into account the naive dimensional analysis and naturalness [23,24,42–44]. For practical purposes, the terms in the Lagrangian are taken up to fourth order in meson-baryon couplings. The baryon-meson interaction is given by [32]

$$\begin{aligned}\mathcal{L} = &\sum_B \overline{\psi}_B\left(i\gamma^\mu D_\mu - m_B + g_{\sigma B}\sigma\right)\psi_B \\ &+\frac{1}{2}\partial_\mu\sigma\,\partial_\mu\sigma - m_\sigma^2\sigma^2\left(\frac{1}{2}+\frac{g_3}{3!}\frac{g_\sigma\sigma}{m_B}+\frac{g_4}{4!}\frac{g_\sigma^2\sigma^2}{m_B^2}\right) \\ &-\frac{1}{4}\Omega_{\mu\nu}\Omega^{\mu\nu}+\frac{1}{2}m_\omega^2\omega_\mu\omega^\mu\left(1+\eta_1\frac{g_\sigma\sigma}{m_B}+\frac{\eta_2}{2}\frac{g_\sigma^2\sigma^2}{m_B^2}\right) \\ &-\frac{1}{4}R^a_{\mu\nu}R^{\mu\nu a}+\frac{1}{2}m_\rho^2\rho^a_\mu\rho^{a\mu}\left(1+\eta_\rho\frac{g_\sigma\sigma}{m_B}\right) \\ &+\frac{1}{4!}\zeta_0(g_\omega\omega_\mu\omega^\mu)^2+\Lambda_v\left(g_\rho^2\rho^a_\mu\rho^{\mu a}\right)\left(g_\omega^2\omega_\mu\omega^\mu\right) \\ &+\sum_l \overline{\psi}_l(i\gamma^\mu\partial_\mu - m_l)\psi_l. \end{aligned} \tag{1}$$

The covariant derivative D_μ is defined as

$$D_\mu = \partial_\mu + ig_\omega\omega_\mu + ig_\rho I_3\tau^a\rho^a_\mu, \tag{2}$$

where $R^a_{\mu\nu}$ and $\Omega_{\mu\nu}$ are field tensors defined as

$$R^a_{\mu\nu} = \partial_\mu\rho^a_\nu - \partial_\nu\rho^a_\mu + g_\rho\mathcal{E}_{abc}\rho^b_\mu\rho^c_\nu, \tag{3}$$

$$\Omega_{\mu\nu} = \partial_\mu\omega_\nu - \partial_\nu\omega_\mu. \tag{4}$$

Here, the symbol B stands for the baryon octet ($n, p, \Lambda, \Sigma^+, \Sigma^0, \Sigma^-, \Xi^-, \Xi^0$) and l represents e^- and μ^-. The masses m_B, m_σ, m_ω, and m_ρ are, respectively, for baryons and for σ, ω, and ρ meson fields. In real calculation, we ignore the non-Abelian term from the ρ field. I_3 is the third component of isospin projection. All symbols carry their own usual meaning [32,45].

For a given Lagrangian density in Eq. (1), one can solve the equations of motion [32,45] in the mean-field level, i.e., the exchange of mesons creates a uniform meson field, where the nucleon has a simple harmonic motion. Then we calculate the energy-momentum tensor within the mean field approximation (i.e., the meson fields are replaced by their classical numbers) and get the EOS as a function of baryon density. The EOS remains uncertain at density larger than the saturation density of nuclear matter, $\rho_n \sim 3\times10^{14}\,\mathrm{g\,cm^{-3}}$. At these densities, neutrons can no longer be considered, which may consist mainly of heavy baryons (mass greater than nucleon) and several other species of particles expected to appear due to the rapid rise of the baryon chemical potentials [46]. The β equilibrium and charge neutrality are two important conditions for the neutron/hyperon-rich matter. Both these conditions force the stars to have ∼90% of neutron and ∼10% proton. With the inclusion of baryons, the β-equilibrium conditions between chemical potentials for different particles are

$$\begin{aligned}\mu_p &= \mu_{\Sigma^+} = \mu_n - \mu_e, \\ \mu_n &= \mu_{\Sigma^0} = \mu_{\Xi^0} = \mu_n, \\ \mu_{\Sigma^-} &= \mu_{\Xi^-} = \mu_n + \mu_e, \\ \mu_\mu &= \mu_e, \end{aligned} \tag{5}$$

and the charge neutrality condition is satisfied by

$$n_p + n_{\Sigma^+} = n_e + n_{\mu^-} + n_{\Sigma^-} + n_{\Xi^-}. \tag{6}$$

The corresponding pressure and energy density of the charge neutral β-equilibrated neutron star matter (which includes the lowest lying octet of baryons) is then given by [32]

$$\begin{aligned}\mathcal{E} = &\sum_B \frac{2}{(2\pi)^3}\int_0^{k_B} d^3k\,E^*_B(k) + \frac{1}{4!}\zeta_0 g_\omega^2\omega_0^4 \\ &+m_\sigma^2\sigma_0^2\left(\frac{1}{2}+\frac{g_3}{3!}\frac{g_\sigma\sigma_0}{m_B}+\frac{g_4}{4!}\frac{g_\sigma^2\sigma_0^2}{m_B^2}\right) \\ &+\frac{1}{2}m_\omega^2\omega_0^2\left(1+\eta_1\frac{g_\sigma\sigma_0}{m_B}+\frac{\eta_2}{2}\frac{g_\sigma^2\sigma_0^2}{m_B^2}\right) \\ &+\frac{1}{2}m_\rho^2\rho_{03}^2\left(1+\eta_\rho+\frac{g_\sigma\sigma_0}{m_B}\right)+3\Lambda_v(g_\rho\rho_{03})^2(g_\omega\omega_0)^2 \\ &+\sum_l \mathcal{E}_l, \end{aligned} \tag{7}$$

and

$$\begin{aligned}P = &\sum_B \frac{2}{3(2\pi)^3}\int_0^{k_B} d^3k\,\frac{k^2}{E^*_B(k)} + \frac{1}{4!}\zeta_0 g_\omega^2\omega_0^4 \\ &-m_\sigma^2\sigma_0^2\left(\frac{1}{2}+\frac{g_3}{3!}\frac{g_\sigma\sigma_0}{m_B}+\frac{g_4}{4!}\frac{g_\sigma^2\sigma_0^2}{m_B^2}\right) \\ &+\frac{1}{2}m_\omega^2\omega_0^2\left(1+\eta_1\frac{g_\sigma\sigma_0}{m_B}+\frac{\eta_2}{2}\frac{g_\sigma^2\sigma_0^2}{m_B^2}\right) \\ &+\frac{1}{2}m_\rho^2\rho_{03}^2\left(1+\eta_\rho\frac{g_\sigma\sigma_0}{m_B}\right)+\Lambda_v(g_\rho\rho_{03})^2(g_\omega\omega_0)^2 \\ &+\sum_l P_l, \end{aligned} \tag{8}$$

where P_l and $\mathcal{E}_l$ are the lepton's pressure and energy density, respectively. $E^*_B = (k_B^2 + M_B^{*2})^{1/2}$ is the effective energy, k_B is the Fermi momentum of the baryons. M^*_p and M^*_n are the proton and neutron effective masses written as

$$M^*_p = M_p - g_\sigma\sigma_0 \tag{9}$$

and

$$M^*_n = M_n - g_\sigma\sigma_0. \tag{10}$$

III. RESULTS AND DISCUSSIONS

In this section, we present the results of our calculations in Figs. 1–9 and Table II. Our calculated results of the equation

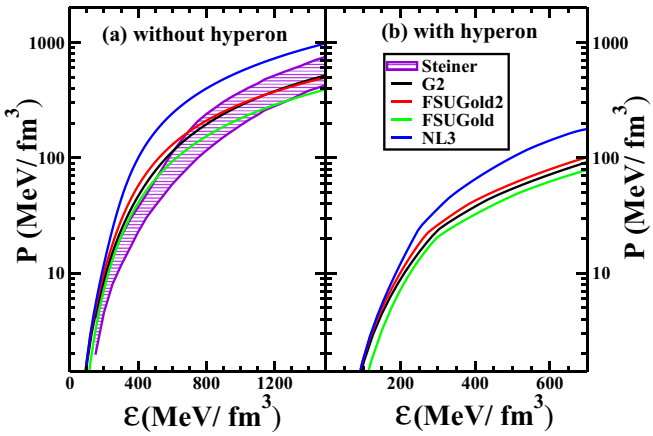

FIG. 1. The equations of state obtained for nuclear and hypernuclear matter under charge neutrality as well as the β-equilibrium condition for G2 [24], FSUGold2 [47], FSUGold [27], and NL3 [37] force parameters are compared with the empirical data [48] (shaded area in the graph) for $r_{ph} = R$ with the uncertainty of 2σ. Here, R and r_{ph} are the neutron radius and the photospheric radius, respectively.

of state and related outputs are discussed in the subsequent subsections.

A. Equations of state

Before going to the estimation of the tidal deformability parameter λ, we check the validity of the EOSs obtained with various well-known force parameters. It is worth mentioning that in Ref. [49], the mass and radius of the hybrid stars with hyperons and quarks are evaluated using the NL3 [37] parameter set. In a relatively recent paper, Bhowmick *et al.* [50] used the FSUGold [27] parameter set to study the properties of hypernuclei for a finite nuclear system [50]. In the present paper, we have used these sets along with FSUGold2 [47] and G2 [24] forces. Although FSUGold2 is relatively new, G2 has a large number of couplings, which are important for various properties of finite and infinite nuclear systems. Figure 1 displays the equation of state for G2 [24], FSUGold2 [47], FSUGold [27], and NL3 [37] parameter sets. From Fig. 1(a), it is obvious that all the EOSs follow a similar trend. Among these four, the celebrity NL3 set gives the stiffest EOS and the relatively new FSUGold represents the softer character. This is because of the large and positive g_4 value as well as the introduction of isoscalar-isovector coupling (Λ) in the FSUGold set [27]. To have an understanding on the softer and stiffer EOSs by various parametrizations, we compared their coupling constants and other parameters of the sets in Table I. We notice a large variation in their effective masses, incompressibilities and other nuclear matter properties at saturation. For higher energy density $\mathcal{E} \sim$ 500–1400 MeV fm^{-3}, except the NL3 set which has the lowest nucleon effective mass, all other sets are found in the region of empirical data with the uncertainty of 2σ [48].

Figure 1(b) shows a hump-type structure on the nucleon-hyperon equation of state at $\mathcal{E}$ around 400–500 MeV fm^{-3}. This kink ($\mathcal{E} \sim$ 200–300 MeV) shows the presence of hyperons in the dense system. Here, the repulsive component of the vector potential becomes more important than the attractive part of the scalar interaction. As a result the coupling of the hyperon-nucleon strength gets weak. At a given baryon density, the inclusion of hyperons significantly lowers the pressure compared to the equation of state without hyperons. This is possible due to the higher energy of the hyperons, as the neutrons are replaced by the low-energy hyperons. The hyperon couplings are expressed as the ratio of the meson-hyperon and meson-nucleon couplings:

$$\chi_\sigma = \frac{g_{Y\sigma}}{g_{N\sigma}}, \quad \chi_\omega = \frac{g_{Y\omega}}{g_{N\omega}}, \chi_\rho = \frac{g_{Y\rho}}{g_{N\rho}}. \tag{11}$$

In the present calculations, we have taken $\chi_\sigma = 0.7$ and $\chi_\omega = \chi_\rho = 0.783$. One can find similar calculations for stellar mass in Refs. [51–54].

TABLE I. Parameters and saturation properties for NL3 [37], G2 [24], FSUGold [27], and FSUGold2 [47]. The parameters g_σ, g_ω, g_ρ, g_3, and g_4 are calculated from nuclear matter given saturation properties using the relations suggested by the authors of Ref. [51].

Parameters	NL3	G2	FSUGold	FSUGold2
m_n(MeV)	939	939	939	939
m_σ(MeV)	508.194	520.206	491.5	497.479
m_ω(MeV)	782.501	782	783	782.5
m_ρ(MeV)	763	770	763	763
g_σ	10.1756	10.5088	10.5924	10.3968
g_ω	12.7885	12.7864	14.3020	13.5568
g_ρ	8.9849	9.5108	11.7673	8.970
g_3(MeV)	1.4841	3.2376	0.6194	1.2315
g_4	–5.6596	0.6939	9.7466	–0.2052
η_1	0	0.65	0	0
η_2	0	0.11	0	0
η_ρ	0	0.390	0	0
ζ_0	0	2.642	12.273	4.705
Λ	0	0	0.03	0.000823
ρ_0(fm^{-3})	0.148	0.153	0.148	0.1505 ± 0.00078
E/A(MeV)	–16.299	–16.07	–16.3	-16.28 ± 0.02
K$_\infty$(MeV)	271.76	215	230	238.0 ± 2.8
J(MeV)	37.4	36.4	32.59	37.62 ± 1.11
L(MeV)	118.2	101.2	60.5	112.8 ± 16.1
m_n^*/m_n	0.6	0.664	0.610	0.593 ± 0.004

B. Mass and radius of neutron star

Once the equations of state for various relativistic forces are fixed, then we extend our study for the evaluation of the mass and radius of the isolated neutron star. The Tolmann-Oppenheimer-Volkov (TOV) equations [55] have to be solved for this purpose, where EOSs are the inputs. The TOV equations are written as

$$\frac{dP(r)}{dr} = -\frac{[\mathcal{E}(r) + P(r)][M(r) + 4\pi r^3 P(r)]}{r^2\left(1 - \frac{2M(r)}{r}\right)} \tag{12}$$

and

$$\frac{dM(r)}{dr} = 4\pi r^2 \mathcal{E}(r). \tag{13}$$

TABLE II. Properties of a $1.4M_\odot$ neutron and hyperon star for a different class of the EOS. The quadrupolar tidal deformability λ and uncertainty error $\Delta\tilde{\lambda}$ in (10^{36} g cm^2 s^2).

EOS	R(km)	C	f_c(Hz)	k_2	k_3	k_4	h_2	h_3	h_4	λ	$\Delta\tilde{\lambda}$	Λ
Neutron star												
NL3	14.422	0.144	1256.7	0.1197	0.0353	0.0142	0.9775	0.6519	0.5074	7.466	2.027	1288.81
G2	13.148	0.157	1440.9	0.0934	0.0265	0.0103	0.8879	0.5951	0.4596	3.668	1.486	652.76
FSUGold2	13.850	0.149	1332.4	0.1040	0.0301	0.0119	0.9275	0.6237	0.4854	5.299	1.763	944.08
FSUGold	12.236	0.170	1608.0	0.0882	0.0244	0.0071	0.8589	0.5634	0.4268	2.418	1.178	414.13
Hyperon star												
NL3	14.430	0.143	1252.9	0.1203	0.0355	0.0143	0.9800	0.6541	0.5096	7.527	2.018	1341.20
G2	12.686	0.163	1520.6	0.0804	0.0229	0.0088	0.8434	0.5707	0.4399	2.641	1.321	465.83
FSUGold2	13.690	0.151	1355.9	0.0988	0.0287	0.0113	0.9108	0.6154	0.4789	4.750	1.696	839.04
$(\text{FSUGold})_{1.3M_\odot}$	9.922	0.194	2119.0	0.0421	0.0116	0.0042	0.6884	0.4683	0.3518	0.4048	0.530	102.14

For a given EOS, the Tolmann-Oppenheimer-Volkov (TOV) equations [55] must be integrated from the boundary conditions $P(0) = P_c$, and $M(0) = 0$, where P_c and $M(0)$ are the pressure and mass of the star at $r = 0$ and the value of $r(= R)$, where the pressure vanish defines the surface of the star. Thus, at each central density we can uniquely determine a mass M and a radius R of the static neutron and hyperon stars using the four chosen EOSs. The estimated results for the maximum mass as a function of radius compared with the highly precise measurements of two massive ($\sim 2M_\odot$) neutron stars [30,31], and the extraction of stellar radii from x-ray observation [48] are shown in Figs. 2(a) and 2(b). From recent observations [30,31], it is clearly illustrated that the maximum mass predicted by any theoretical models should reach the limit $\sim 2.0M_\odot$, which is consistent with our present prediction from the G2 equation of state of a nucleonic matter compact star with mass $1.99M_\odot$ and radius 11.25 km. From x-ray observations, Steiner *et al.* [48] predicted that the most-probable neutron star radii lie in the range 11–12 km with neutron star masses

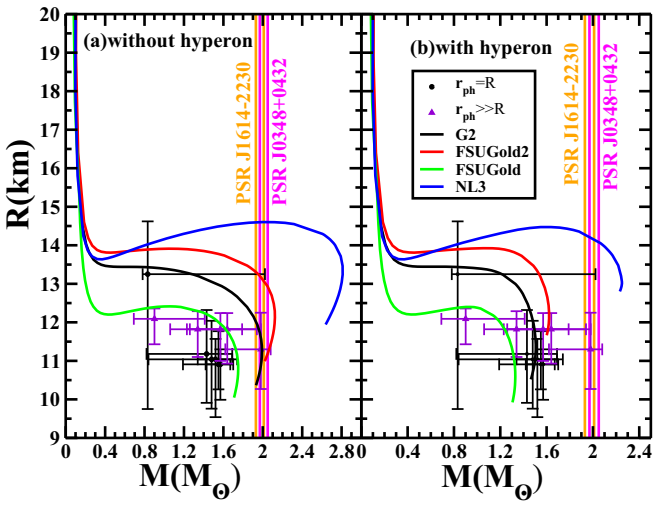

FIG. 2. The mass-radius profile for the force parameters like G2 [24], FSUGold2 [47], FSUGold [27], and NL3 [37] used. The solid circles ($r_{ph} = R$) and triangles ($r \gg R$) represent the observational constraints [48], where r_{ph} is the photospheric radius. The vertical shaded region corresponds to the recent observation [30,31].

$\sim 1.4M_\odot$ and predicted the EOS is relatively soft in the density range 1–3 times the nuclear saturation density. As explained earlier, stiff EOS-like NL3 predicts a larger stellar radius 13.23 km and a maximum mass 2.81 $M_\odot$. Though FSUGold and FSUGold2 are from the same RMF model with similar terms in the Lagrangian, their results for a neutron star are quite different with FSUGold2 suggesting a larger and heavier NS with mass $2.12M_\odot$ and radius 12.12 km compared to the mass and radius ($1.75M_\odot$ and 10.76 km) of the FSUGold. Because in FSUGold2 EOS at high densities, the impact comes from the quartic vector coupling constant ζ_0 and also the large values of the slope parameter $L = 112.8 \pm 16.1$ MeV (see Table I) tend to predict the neutron star with large radius [56]. From the observational point of view, there are large uncertainties in the determination of the radius of the star [57–59], which is a hindrance to get a precise knowledge on the composition of the star atmosphere. One can see that the G2 parameter is able to reproduce the recent observation of $2.0M_\odot$ NS. But the presence of hyperon matter under β equilibrium softens the EOS, because they are more massive than nucleons and when they start to fill their Fermi sea slowly replacing the highest energy nucleons. Hence, the maximum mass of NS is reduced by ~ 0.5 unit solar mass due to the high baryon density. For example, the stiffer NL3 equation of state gives the maximum NS mass $\sim 2.81M_\odot$ and the presence of hyperon matter reduces the mass to $\sim 2.25M_\odot$ as shown in Fig. 2(b). These results give us warning that most of the present sets of hyperon couplings are unable to reproduce the recently observed mass of neutron star like PSR J1614-2230 with mass $M = 1.97 \pm 0.04M_\odot$ [30] and the PSR J0348+0432 with $M = 2.01 \pm 0.04M_\odot$ [31]. Probably, this suggests to us to modify the coupling constants and get the equations of state properly, so that one can explain all the mass-radius observations to date. Further, one can see that in Fig. 2(b) the mass-radius curve of G2, FSUGold, FSUGold2 with hyperon lies in the range of the predicted equation of state between the $r_{ph} = R$ and $r_{ph} \gg R$ cases is the high density behavior [48].

C. Various tidal Love numbers of compact stars

When a spherical star is placed in a static external quadrupolar tidal field $\mathcal{E}_{ij}$ then the star will be deformed and quadrupole deformation will be the leading order perturbation.

Such a deformation is defined as the ratio of the mass quadrupole moment of a star Q_{ij} to the external tidal field $\mathcal{E}_{ij}$:

$$\lambda = -\frac{Q_{ij}}{\mathcal{E}_{ij}}. \tag{14}$$

Specifically, the observable of the tidal deformability parameter λ depends on the EOS via both the neutron star (NS) radius and a dimensionless quantity k_2, called the Love number and is given by the relation

$$\lambda = \tfrac{2}{3}k_2 R^5, \tag{15}$$

and the dimensionless tidal-deformability (Λ) is related with the compactness parameter $C = M/R$ as

$$\Lambda = \frac{2k_2}{3C^5}, \tag{16}$$

where R is the radius of the (spherical) star in isolation. Now, we have to get k_2 for the calculation of the deformability parameter λ, which is the key quantity of deformation due to the gravitational attraction of the binary stars with each other. This force of attraction becomes more and more important in the course of time, because of the reduction of the orbital distance between them. The orbital distance between the binary decreases as the companion star emits gravitational radiation. As a result, the binary accelerates and finally merges with each other and possibly turns to a black hole. Thus, the estimation of the leading order quadrupole electric tidal Love number k_2 along with other higher order Love numbers k_3 and k_4 is very important for the detection of gravitational wave.

To estimate the Love numbers k_l ($l = 2, 3, 4$), along with the evaluation of the TOV equations, we have to compute $y = y_l(R)$ with initial boundary condition $y(0) = l$ from the following first-order differential equation iteratively [5,6,18,60]:

$$r\frac{dy(r)}{dr} + y(r)^2 + y(r)F(r) + r^2Q(r) = 0 \tag{17}$$

with

$$F(r) = \frac{r - 4\pi r^3[\mathcal{E}(r) - P(r)]}{r - 2M(r)}, \tag{18}$$

$$Q(r) = \frac{4\pi r\left(5\mathcal{E}(r) + 9P(r) + \frac{\mathcal{E}(r)+P(r)}{\partial P(r)/\partial \mathcal{E}(r)} - \frac{l(l+1)}{4\pi r^2}\right)}{r - 2M(r)} - 4\left[\frac{M(r) + 4\pi r^3 P(r)}{r^2(1 - 2M(r)/r)}\right]^2. \tag{19}$$

Once we know the value of $y = y_l(R)$, the electric tidal Love numbers k_l are found from the following expression [60]:

$$k_2 = \frac{8}{5}(1-2C)^2C^5[2C(y_2-1) - y_2 + 2]\Big\{2C(4(y_2+1)C^4 + (6y_2-4)C^3 + (26-22y_2)C^2 + 3(5y_2-8)C - 3y_2 + 6) - 3(1-2C)^2(2C(y_2-1) - y_2 + 2)\log\left(\frac{1}{1-2C}\right)\Big\}^{-1}, \tag{20}$$

$$k_3 = \frac{8}{7}(1-2C)^2C^7[2(y_3-1)C^2 - 3(y_3-2)C + y_3 - 3]\Big\{2C[4(y_3+1)C^5 + 2(9y_3-2)C^4 - 20(7y_3-9)C^3 + 5(37y_3-72)C^2 - 45(2y_3-5)C + 15(y_3-3)] - 15(1-2C)^2(2(y_3-1)C^2 - 3(y_3-2)C + y_3 - 3)\log\left(\frac{1}{1-2C}\right)\Big\}^{-1}, \tag{21}$$

and

$$k_4 = \frac{32}{147}(1-2C)^2C^9[12(y_4-1)C^3 - 34(y_4-2)C^2 + 28(y_4-3)C - 7(y_4-4)]\Big\{2C[8(y_4+1)C^6 + (68y_4-8)C^5 + (1284-996y_4)C^4 + 40(55y_4-116)C^3 + (5360-1910y_4)C^2 + 105(7y_4-24)C - 105(y_4-4)] - 15(1-2C)^2[12(y_4-1)C^3 - 34(y_4-2)C^2 + 28(y_4-3)C - 7(y_4-4)]\log\left(\frac{1}{1-2C}\right)\Big\}^{-1}. \tag{22}$$

As we have emphasized earlier, the dimensionless Love number k_l ($l = 2, 3, 4$) is an important quantity to measure the internal structure of the constituent body. These quantities directly enter into the gravitational wave phase of an inspiraling binary neutron star (BNS) and extract the information of the EOS. Notice that Eqs. (20)–(22) contain an overall factor $(1-2C)^2$, which tends to zero when the compactness approaches the compactness of the black hole, i.e., $C^{BH} = 1/2$ [61]. Also, it is to be pointed out that with the presence of multiplication order factor C with $(1-2C)^2$ in the expression of k_l that the value of the Love number of a black hole simply becomes zero, i.e., $k_l^{BH} = 0$.

Figure 3 shows the tidal Love numbers k_l ($l = 2, 3, 4$) as a function ofcompactness parameter C for the neutron star with four selected EOSs. The result of k_l suddenly decreases with increasing compactness ($C = 0.06$–0.25). For each EOS, the value of k_2 appears to be a maximum between $C = 0.06$–0.07. However, we are mainly interested in the neutron star masses at $\sim 1.4M_\odot$. Because of the tidal interactions in the neutron star binary, the shape of the star acquires quadrupole, octupole, hexadecapole, and other higher-order deformations. The value of the Love numbers for corresponding shapes are shown in Table II. The values of k_l decrease gradually with an increase of multipole moments. Thus, the quadrupole deformability

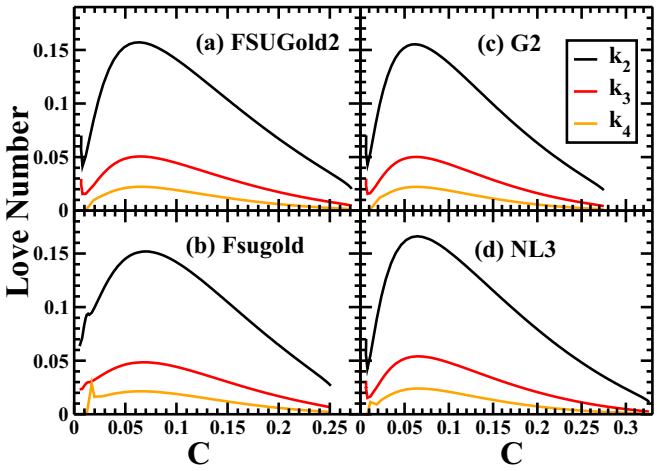

FIG. 3. The tidal Love numbers k_2, k_3, k_4 as a function of the mass of the four selected EOSs of the neutron star.

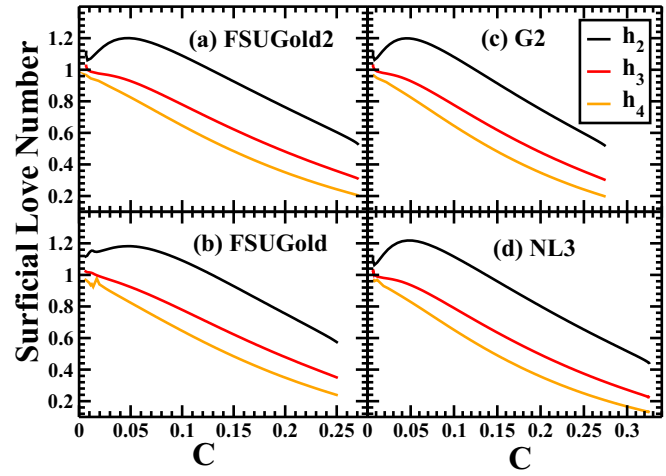

FIG. 5. Surficial Love number h_l as a function of compactness C of a neutron star, for selected values of l.

has maximum effects on the binary star merger. Similarly, in Fig. 4, the dimensionless Love number k_l is shown as a function of compactness for the hyperon star. With the inclusion of hyperons, the effect of the core is negligible due to the softness of the EOSs. The values of k_l are different for a typical neutron-hyperon star with 1.4 $M_\odot$ for various sets listed in the lower portion of Table II. The radius and respective mass-radius ratio are also given in Table II. The table also reflects that the Love numbers decrease slightly or remain unchanged with the addition of a hyperon in the neutron star. The neutron star surface or solid crust is not responsible for any tidal effects, but instead it is the matter mainly in the outer core that gives the largest contribution to the tidal Love numbers. It is relatively unaffected by changing the composition of the core and leave it at that. Thus it instigates the calculation for the surficial Love number h_l for both neutron and hyperon star binary.

Next, we calculate the surficial Love number h_l which describes the deformation of the body's surface in a multipole expansion. Recently, Damour and Nagar [61] have given the surficial Love number (also known as shape Love number) h_l

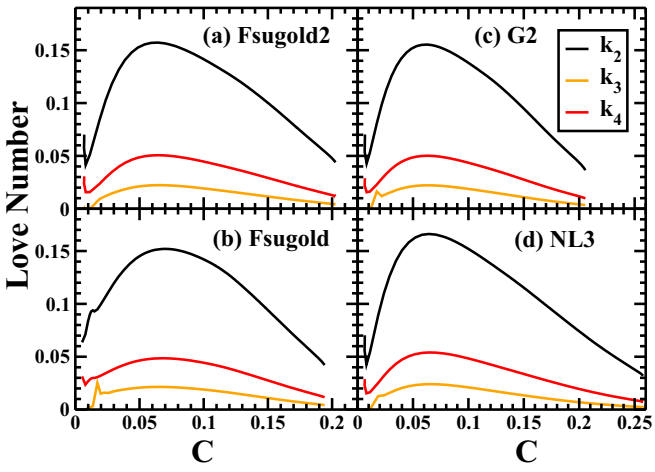

FIG. 4. Same as Fig. 3 but for hyperon star.

for the coordinate displacement δR of the body's surface under the external tidal force. Alternatively, Landry and Poisson [19] have proposed the definition of the Newtonian Love number in terms of a curvature perturbation $\delta\mathcal{R}$ instead of a surface displacement δR. For a perfect fluid, the relation between the surficial Love number h_l and tidal Love number k_l is given as

$$h_l = \Gamma_1 + 2\Gamma_2 k_l, \tag{23}$$

$$\Gamma_1 = \frac{l+1}{l-1}(1-C)F(-l,-l,-2l;2C) - \frac{2}{l-1}F(-l,-l-1,-2l;2C),$$

$$\Gamma_2 = \frac{l}{l+2}(1-C)F(l+1,l+1,2l+2;2C) + \frac{2}{l+2}F(l+1,l,2l+2;2C), \tag{24}$$

where $F(a,b,c;z)$ is the hypergeometric function. Figure 5 shows the results of surficial Love number h_l of a neutron star as a function of compactness parameter C. Unlike the initially increasing and then decreasing trend of the tidal Love number k_l, the surficial Love number h_l decreases almost exponentially with the compactness parameter. At the minimum value of the compactness parameter, the maximum value of the shape Love number of each multipole moment approaches 1. Thus, we zero in on to the Newtonian relation, i.e., $h_l = 1 + 2k_l$. Again one can compute from Table II that the surficial Love number h_l decreases ~20% from one moment to another. For example, $h_2 = 0.9775$ and $h_3 = 0.6519$ and $h_4 = 0.5074$ for NL3 parameter sets.

Furthermore, we also calculate the "magnetic" tidal Love number j_l. Here, we give only the quadrupolar case ($l = 2$), which is expressed as

$$j_2 = \{96C^5(2C-1)(y_2-3)\}\{5(2C(12(y_2+1)C^4 + 2(y_2-3)C^3 + 2(y_2-3)C^2 + 3(y_2-3)C - 3y_2 + 9) + 3(2C-1)(y_2-3)\log(1-2C))\}^{-1}. \tag{25}$$

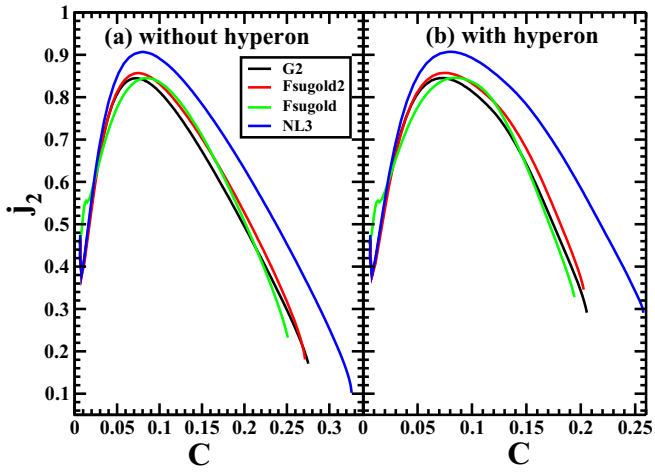

FIG. 6. The magnetic tidal Love number for selected EOSs.

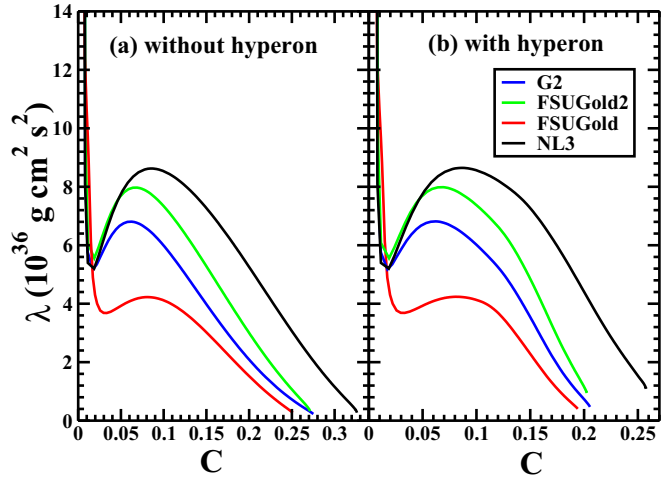

FIG. 7. The tidal deformability λ as a function of the compactness C for the four EOS with and without hyperon.

After inserting the value of y_2 in Eq. (25), we compute the magnetic tidal Love number j_2 in a hydrostatic equilibrium condition for a nonrotating neutron star. This gives important information about the internal structure [18] without changing the tidal Love number k_2. At $C = 0.01$, the magnetic Love number j_2 is nearly 0.4. In both cases (with and without hyperons), j_2 is maximum within the compactness 0.06 to 0.07 for all the four EOSs (see Fig. 6). Then the value of j_2 decreases sharply with an increase of compactness. The NL3 parameter set gives a maximum j_2 in both systems, while the rest of the three sets predict a comparable j_2.

D. Tidal deformability and cut-off frequency of compact star

From Eq. (15), it is known that the tidal deformability λ is a function of the linear tidal Love number k_2 and the fifth power of the radius R^5 of the compact star. For this purpose, we solve numerically Eqs. (12)–(20) using the initial boundary condition. To examine the results of tidal deformability with and without hyperons, we have shown the $\lambda - C$ plot in Fig. 7, where we have considered a single neutron star under the influence of an external tidal field with an adiabatic approximation using the four equations of state. In this case, the orbital evaluation time scale is much larger than the time scale needed to assume the star as a stationary configuration. From the very beginning, we mark an infinitely large λ corresponding to a small compactness, i.e., $C \sim 0.02$. Further, the λ value falls to a minima that rises again resulting in a hump-like pattern for each EOS. It is noteworthy that in Fig. 7(b) by introducing the NL3 case with hyperon, there is a remarkable but mere deviation in λ value, i.e., $7.527\,\mathrm{g\,cm^2\ s^2}$ (without hyperon $\lambda = 7.466\,\mathrm{g\,cm^2\ s^2}$). Since, the tidal deformability λ is a surface phenomenon, it is very much getting affected by the radius of the star in both normal neutron star and hyperon star. Thus, the tidal deformability λ becomes highly sensitive on the radius R even though k_2 is small. We estimate the radii to be within 12.236–14.422 km for a neutron star of mass $1.4M_\odot$ and the range is 13.690–14.430 km for neutron-hyperon star for all the four stiff or soft equations of state (see Table II).

Figure 8 shows the tidal deformability for both neutron and hyperon stars. We have a large radii for a smaller stellar mass of $\sim 0.1M_\odot$ in both cases. At this value of mass and radius, the tidal deformability λ becomes maximum, because for a large radius with smaller mass, the force of attraction within the star is weak and when another star comes closer, the gravitational pull overrides a maximum at the surface part of the star. This phenomenon is true for both neutron as well as hyperon stars [5,6]. Then, suddenly the tidal deformability decreases and again increases as shown in the figure making a broad peak at around $M = 0.7$–$0.8M_\odot$ and then decreases smoothly with an increase in the mass of the star. Since, the tidal deformability depends a lot on both the mass and radius of a neutron star, it is imperative to measure the radius of the star precisely, as the mass is already measured with very

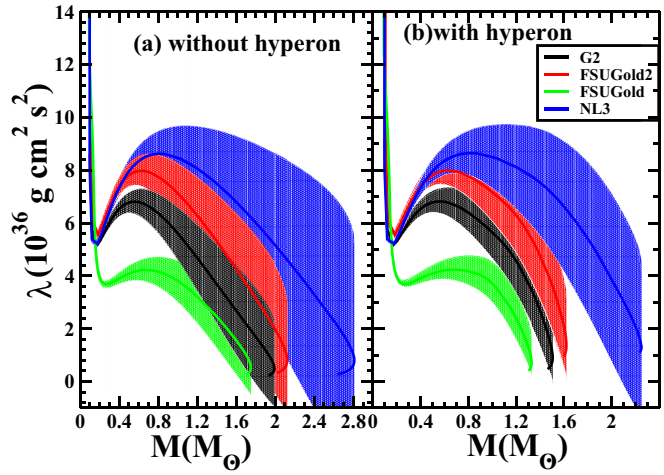

FIG. 8. Tidal deformability λ of a single neutron star as a function of the neutron-star mass for a range of EOSs. The estimate of uncertainties in measuring λ for equal mass binaries at a distance of $D = 100$ Mpc is shown for the advanced LIGO detector in shaded area. (b) Same as (a), but for hyperon star.

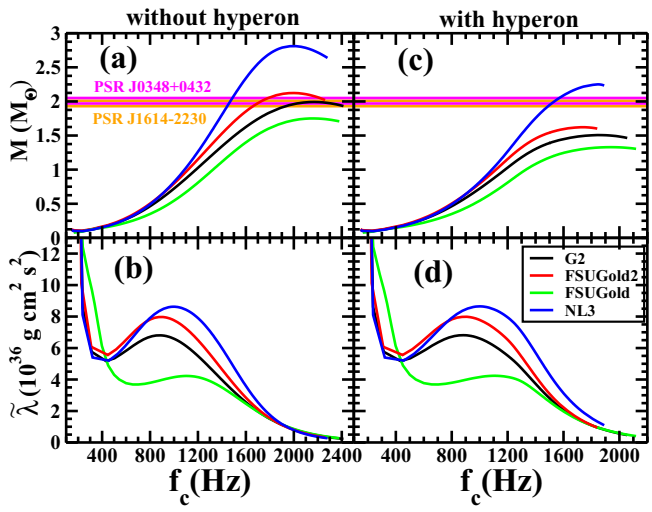

FIG. 9. (a), (c) The mass cut-off frequency f_c profile of normal and hyperon stars using four EOSs. (b) The tidal deformability with cut-off frequency plot of the neutron star. (d) Same as (b), but for hyperon star.

good precession. Recently, Steiner *et al.* predicted the most extreme limit for the tidal deformabilities between 0.6 and 6 $\times$ 10^{36} g cm^2 s^2 for $1.4M_\odot$ with 95% confidence. This range can be constrained on high dense matter of any measurements [62]. Mostly, the binaries masses are about $1.4M_\odot$, so in particular we are interested in studying the phenomena within this mass range and the results are summarized in Table II. Comparing the results, we notice that the tidal deformability λ is quite sensitive to the EOS. It is more for stiffer EOS, because of the high-density behavior of the symmetry energy [63].

Finally, we calculate the weighted tidal deformability of the binary neutron star of mass m_1 and m_2 and it approximately is [5,6]

$$\tilde{\lambda} = \frac{1}{26}\left[\frac{m_1 + 12m_2}{m_1}\lambda_1 + \frac{m_2 + 12m_1}{m_2}\lambda_2\right], \qquad (26)$$

and the root mean square (rms) measurement uncertainty $\Delta\tilde{\lambda}$ can be calculated following the approximate formula [5,6]:

$$\Delta\tilde{\lambda} \approx \alpha\left(\frac{M}{M_\odot}\right)^{2.5}\left(\frac{m_2}{m_1}\right)^{0.1}\left(\frac{f_{\rm cut}}{\rm Hz}\right)^{-2.2}\left(\frac{D}{100\,\rm Mpc}\right), \qquad (27)$$

where $\alpha = 1.0 \times 10^{42}\,\mathrm{g\,cm^2\ s^2}$ is the tidal deformability for a single advanced LIGO detector and $f_{\rm cut}$ ($f_{\rm end}$) cutoff frequency [12] for the end stage of the inspiral binary neutron stars. D denotes the luminosity distance from the source to observer.

The weighted tidal deformability for neutron and hyperon stars and their corresponding masses as cut-off frequency $f_{\rm cut}$ are shown in Fig. 9. The cut-off frequency is a stopping criterion to estimate when the tidal model no longer describes the binary. Here, we take the cut-off to be approximately when the two neutron stars come into contact, estimated as in Eq. (36) of Ref. [12]. Specifically, we use $f_{\rm cut} = 2f_{\rm orb.}^{N(R_1+R_2)}$, where $f_{\rm orb.}^{N(R_1+R_2)}$ is the Newtonian orbital frequency corresponding to the orbital separation where two unperturbed neutron stars with radii R_1 and R_2 would touch. In Fig. 9(a), 9(c), it shows the variation of mass of the binary as a function of cut-off frequency $f_{\rm cut}$. Here, we considered $m_1 = m_2$, i.e., both the masses of the binary are equal. Initially, the masses of the stars $0.2M_\odot$ remain almost constant up to $f_{\rm cut} \approx 400$ Hz. Then the mass increases nearly exponentially up to a maximum mass of ≈ 1.75–$2.81M_\odot$ (for NS) and ≈ 1.33–$2.25M_\odot$ (for hyperon star) and then decreases. By this time, the cut-off frequency $f_{\rm cut}$ attains quite a large value. When the individual mass of the binary is $1.4M_\odot$, the NL3 set weighted tidal deformability achieves the cut-off frequency $f_{\rm cut} \approx 1256.7$ Hz as the minimum contrary to the $f_{\rm cut} \approx 1608.0$ Hz of FSUGold at the same mass of the single NS. It is also clear from the figure that the weighted tidal deformabilities of the NS for the four models are 7.466, 3.668, 5.229, and 2.418 for NL3, G2, FSUGold2, and FSUGold, respectively, with the corresponding frequency 1256.7, 1440.9, 1332.4, and 1608.0 Hz.

Using the cut-off frequency, we calculate the uncertainty in the measurement of the tidal deformability ($\Delta\tilde{\lambda}$) obtained from these four EOSs for an equal-mass binary star inspiral at 100 Mpc from aLIGO detector (shaded region in Fig. 8). The uncertainty in the lower mass region (0.4–$1.0M_\odot$) of the NS $\Delta\tilde{\lambda}$ is smaller. Similar results are found in the case of the hyperon star also. Interestingly, the error ($\Delta\tilde{\lambda}$) increases with an increase in the mass of the binary for all the EOSs. From Table II, by comparing the $\Delta\tilde{\lambda}$ obtained from all the EOSs, we find that predicted errors are greater than the measured value for a star of mass $1.4M_\odot$.

IV. SUMMARY AND CONCLUSIONS

In summary, four different models have been extensively applied which are obtained from an effective field theory motivated relativistic mean field formalism. This effective interaction model satisfies the nuclear saturation properties and reproduce the bulk properties of finite nuclei with a very good accuracy. We used these four forces of interaction and calculate the equations of state for neutron and hyperon star matter. It is noteworthy that each term of the interaction has its own meaning and has specific character. The inclusion of extra terms (nucleons replaced by baryons octet) in the Lagrangian contribute to soften the EOS and the matter becomes less compressible. Hence, there is a decrease in the maximum mass by $\sim 0.5M_\odot$ than the pure neutron star.

We have extended our calculations to various tidal responses both for electric-types (even-parity) and magnetic-types (odd-parity) of neutron and hyperon stars in the influence of an external gravitational tidal field. The Love numbers are directly connected with surficial Love number h_l associated with the surface properties of the stars. Subsequently, we study the quadrupolar tidal deformability λ of normal neutron star and hyperon star using a different set of equation of state. These tidal deformabilities particularly depend on the quadrupole Love number k_2 and radius (R) of the isolated star. Although the maximum value of k_2 is not very sensitive to the EOS for neutron and hyperon stars lying in the range $k_2 \approx 0.144$–0.170 and 0.143–0.194 for neutron and hyperon stars, respectively, but it is very much sensitive to the radius of the star.

We find that aLIGO can constrain on the existence of hyperon star, i.e., the inner core of the NS has hyperons, but detecting them can be much harder. However, it should be able to constrain the neutron star deformability to $\lambda \leqslant 10 \times 10^{36}\,\mathrm{g\,cm^2\ s^2}$ for a binary of $1.4M_\odot$ neutron stars at a distance 100 Mpc from the detector. In the future, we expect that aLIGO should be able to measure λ even for neutron stars masses up to $2.0M_\odot$ and consequently constrain the stiffness of the equations of state. It is worth mentioning that the present calculations are based on the extrapolation of the formula $\Delta\tilde{\lambda}$ given in Refs. [5,64,65]. Here, the systematic uncertainties in the model that was used to obtain the measurability estimates are neglected.

ACKNOWLEDGMENTS

Bharat Kumar would like to take this opportunity to convey special thanks to Dr. Tanja Hinderer for her keen interest, fruitful discussions, and useful suggestions.

[1] B. P. Abbott *et al.*, Phys. Rev. Lett. **116**, 061102 (2016); LIGO, www.ligo.caltech.edu.
[2] VIRGO, www.virgo.infn.it.
[3] Kagra, http://gwcenter.icrr.u-tokyo.ac.jp/en/.
[4] É. É. Flanagan and T. Hinderer, Phys. Rev. D **77**, 021502 (2008).
[5] T. Hinderer, Astrophys. J. **677**, 1216 (2008); **697**, 964 (2009).
[6] T. Hinderer, B. D. Lackey, R. N. Lang, and J. S. Read, Phys. Rev. D **81**, 123016 (2010).
[7] L. Baiotti, T. Damour, B. Giacomazzo, A. Nagar, and L. Rezzolla, Phys. Rev. Lett. **105**, 261101 (2010).
[8] L. Baiotti, T. Damour, B. Giacomazzo, A. Nagar, and L. Rezzolla, Phys. Rev. D **84**, 024017 (2011).
[9] J. Vines, É. É. Flanagan, and T. Hinderer, Phys. Rev. D **83**, 084051 (2011).
[10] F. Pannarale, L. Rezzolla, F. Ohme, and J. S. Read, Phys. Rev. D **84**, 104017 (2011).
[11] B. D. Lackey, K. Kyutoku, M. Shibata, P. R. Brady, and J. L. Friedman, Phys. Rev. D **85**, 044061 (2012).
[12] T. Damour, A. Nagar, and L. Villain, Phys. Rev. D **85**, 123007 (2012).
[13] J. S. Read, L. Baiotti, J. D. E. Creighton, J. L. Friedman, B. Giacomazzo, K. Kyutoku, C. Markakis, L. Rezzolla, M. Shibata, and K. Taniguchi, Phys. Rev. D **88**, 044042 (2013).
[14] J. E. Vines and É. É. Flanagan, Phys. Rev. D **88**, 024046 (2013).
[15] B. D. Lackey, K. Kyutoku, M. Shibata, P. R. Brady, and J. L. Friedman, Phys. Rev. D **89**, 043009 (2014).
[16] M. Favata, Phys. Rev. Lett. **112**, 101101 (2014).
[17] A. E. H. Love, *Some Problems of Geodynamics* (Cornell University Library, Ithaca, NY, 1911).
[18] T. Binnington and E. Poisson, Phys. Rev. D **80**, 084018 (2009).
[19] P. Landry and Eric Poisson, Phys. Rev. D **89**, 124011 (2014).
[20] P. G. Reinhard, Rep. Prog. Phys. **52**, 439 (1989).
[21] P. Ring, Prog. Part. Nucl. Phys. **37**, 193 (1996).
[22] J. D. Walecka, Ann. Phys. (NY) **83**, 491 (1974).
[23] R. J. Furnstahl, B. D. Serot, and H. B. Tang, Nucl. Phys. A **598**, 539 (1996).
[24] R. J. Furnstahl, B. D. Serot, and H. B. Tang, Nucl. Phys. A **615**, 441 (1997).
[25] J. Boguta and A. R. Bodmer, Nucl. Phys. A **292**, 413 (1977).
[26] A. R. Bodmer, Nucl. Phys. A **526**, 703 (1991).
[27] B. G. Todd-Rutel and J. Piekarewicz, Phys. Rev. Lett. **95**, 122501 (2005).
[28] Y. Sugahara and H. Toki, Nucl. Phys. A **579**, 557 (1994).
[29] R. Machleidt, K. Holinde, and Ch. Elster, Phys. Rep. **149**, 1 (1987).
[30] P. B. Demorest, T. Pennucci, S. M. Ransom, M. S. E. Roberts, and J. W. T. Hessels, Nature (London) **467**, 1081 (2010).
[31] J. Antoniadis *et al.*, Science **340**, 6131 (2013).
[32] B. K. Sharma, P. K. Panda, and S. K. Patra, Phys. Rev. C **75**, 035808 (2007).
[33] P. G. Reinhard, M. Rufa, J. Maruhn, W. Greiner, and J. Friedrich, Z. Phys. A **323**, 13 (1986).
[34] Y. K. Gambhir, P. Ring, and A. Thimet, Ann. Phys. (NY) **198**, 132 (1990).
[35] P. G. Reinhard, Z. Phys. A **329**, 257 (1988).
[36] M. M. Sharma, G. A. Lalazissis, and P. Ring, Phys. Lett. B **312**, 377 (1993).
[37] G. A. Lalazissis, J. Konig, and P. Ring, Phys. Rev. C **55**, 540 (1997).
[38] M. Oka, K. Shimizu, and K. Yazaki, Nucl. Phys. A **464**, 700 (1987).
[39] C. Nakamoto, Y. Suzuki, and Y. Fujiwara, Prog. Theor. Phys. **94**, 65 (1995).
[40] C. Nakamoto, Y. Suzuki, and Y. Fujiwara, Prog. Theor. Phys. **97**, 761 (1997).
[41] C. Nakamoto and Y. Suzuki, Phys. Rev. C **94**, 035803 (2016).
[42] H. Müller and B. D. Serot, Nucl. Phys. A **606**, 508 (1996).
[43] R. J. Furnstahl and B. D. Serot, Nucl. Phys. A **671**, 447 (2000).
[44] R. Machleidt and D. R. Entem, Phys. Rep. **503**, 1 (2011).
[45] S. K. Singh, S. K. Biswal, M. Bhuyan, and S. K. Patra, Phys. Rev. C **89**, 044001 (2014).
[46] M. Baldo, G. F. Burgio, and H.-J. Schulze, Phys. Rev. C **61**, 055801 (2000).
[47] W.-C. Chen and J. Piekarewicz, Phys. Rev. C **90**, 044305 (2014).
[48] A. W. Steiner, J. M. Lattimer, and E. F. Brown, Astrophys. J. **722**, 33 (2010).
[49] L. Bonanno and A. Sedrakian, Astron. Astrophys. **539**, A16 (2012).
[50] B. Bhowmick, A. Bhattacharya, and G. Gangopadhyay, Int. J. Mod. Phys. E **21**, 1250069 (2012).
[51] N. K. Glendenning, *Compact Stars*, 2nd ed. (Springer, New York, 2000).
[52] A. L. Espíndola and D. P. Menezes, Phys. Rev. C **65**, 045803 (2002).
[53] S. Weissenborn, D. Chatterjee, and J. Schaffner-Bielich, Nucl. Phys. A **881**, 62 (2012); Phys. Rev. C **85**, 065802 (2012).
[54] L. L. Lopes and D. P. Menezes, Phys. Rev. C **89**, 025805 (2014).
[55] J. R. Oppenheimer and G. M. Volkoff, Phys. Rev. **55**, 374 (1939); R. C. Tolman, *ibid.* **55**, 364 (1939).
[56] C. J. Horowitz and J. Piekarewicz, Phys. Rev. C **64**, 062802 (2001).

[57] R. Rutledge, L. Bildsten, E. Brown, G. Paplov, and V. Zavlin, Astrophys. J. **577**, 346 (2002); **578**, 405 (2002).
[58] B. Gendre, D. Barret, and N. A. Webb, Astron. Astrophys. **400**, 521 (2003); W. Becker *et al.*, Astrophys. J. **594**, 364 (2003).
[59] J. Cottam, F. Paerels, and M. Mendez, Nature (London) **420**, 51 (2002).
[60] T. Damour and A. Nagar, Phys. Rev. D **81**, 084016 (2010).
[61] T. Damour and A. Nagar, Phys. Rev. D **80**, 084035 (2009).
[62] A. W. Steiner, S. Gandolfi, F. J. Fattoyev, and W. G. Newton, Phys. Rev. C **91**, 015804 (2015).
[63] F. J. Fattoyev, J. Carvajal, W. G. Newton, and B. A. Li, Phys. Rev. C **87**, 015806 (2013).
[64] Leslie Wade, Jolien D. E. Creighton, Evan Ochsner, Benjamin D. Lackey, Benjamin F. Farr, Tyson B. Littenberg, and Vivien Raymond, Phys. Rev. D **89**, 103012 (2014).
[65] LSC Algorithm Llibrary, http://www.lscgroup.phys.uwm.edu/lal.